

Research Paper

Laboratory investigation on morphology response of submerged artificial sandbar and its impact on beach evolution under storm wave condition

Yuan Li ^{a,b}, Chi Zhang ^{a,b,*}, Weiqi Dai ^c, Dake Chen ^b, Titi Sui ^{b,*}, Mingxiao Xie ^{d,*}, Songgui Chen ^d

^a State Key Laboratory of Hydrology-Water Resources and Hydraulic Engineering, Hohai University, Nanjing 210098, China

^b College of Harbour, Coastal and Offshore Engineering, Hohai University, Nanjing 210098, China

^c Yellow River Institute of Hydraulic Research, Yellow River Conservancy Commission (YRCC), Zhengzhou 450000, China

^d Tianjin Research Institute of Water Transport Engineering, Tianjin, 300456, China

ARTICLE INFO

Editor: Shu Gao

Keywords:

Beach nourishment
Submerged Artificial Sandbar
Morphology evolution
Sediment transport
Morphological coupling
Wave energy dissipation

ABSTRACT

The Submerged Artificial sandBar (SAB), recognized as one of the nature-based solutions for beach protection and restoration, has become increasingly popular in coastal engineering applications. However, its morphological response to waves and the resulting impacts on beach evolution are yet not well understood. Here, laboratory experiments are conducted considering different background profiles and various SAB designs. Morphological evolution of the SAB and berm are inspected from the measured beach profile data in the wave flume. Results show that the SAB migrates onshore with its bar shape decaying, providing a paradigm shift away from the traditional understanding that the net subaqueous sediment transport is always offshore directed under storm wave conditions. SAB can alter the beach state and berm behavior by triggering onshore sediment transport locally and temporarily. The stability of the SAB is controlled by its seaward slope and the ratio of crest water depth to the bar height. A morphological coupling is found between the SAB and berm, and an empirical relationship is proposed to quantitatively capture it. Finally, the experiment results are used to validate a process-based beach profile evolution numerical model, and an explanation for the morphological coupling is provided from the perspective of wave energy dissipation.

1. Introduction

Under the impact of climate changes (e.g., increasing sea level, varying wave height, magnitude and frequency of storms), nowadays beach erosion is a worldwide problem affecting the safety of coastal areas (e.g., Camus et al., 2017; Toimil et al., 2020; Voudoukis et al., 2018), and beach protection has become one of the most crucial issues. Severe beach erosion and inundation are more likely to occur under storm wave conditions, which have become frontier research issues in terms of coastal hydrodynamics and morphodynamics (e.g., Baldock et al., 2021; Dissanayake et al., 2015; Eichendorf et al., 2019, 2020a; Xing et al., 2021; Zheng et al., 2020). Recently, the shoreface nourishment has emerged as an environmental-friendly alternative to traditional engineering protection approaches such as the detached breakwaters or groins (e.g., de Schipper et al., 2020; Fan et al., 2021; Hamm et al., 2002; Luo et al., 2015; Liu et al., 2019a, 2019b; Schoonees et al., 2019; Zhu and Kobayashi, 2021).

The shoreface nourishment is usually conducted by filling sediment of similar properties on the intertidal shoreface to form Submerged Artificial sandBar (hereafter SAB), which has been proved effective in reducing beach erosion (e.g., Cooke et al., 2012; Liu et al., 2019a, 2019b). The SAB has two functions in the sense of beach protection, namely the lee-effect and feeder-effect. The lee-effect is shown as large waves tend to break over the SAB, resulting in a decrease in sediment concentration and sediment transport capacity in the covered areas. Besides, the SAB (functioning as a feeder) can provide additional sand supply to the existing bar-beach unit. The lee-effect is recognized as the main protective mechanism for the beach or dune during erosion events, while the feeder-effect plays a more important role in accretion events.

The SAB usually has steep slopes and small water depth over its crest, which may not adapt to the local hydrodynamics. This indicates the morphological evolution of the SAB should involve complicated wave-current-sediment interactions. A considerable amount of field studies on shoreface nourishment evolution have been conducted. Grunnet and

* Corresponding author at: State Key Laboratory of Hydrology-Water Resources and Hydraulic Engineering, Hohai University, Nanjing 210098, China.

E-mail addresses: zhangchi@hhu.edu.cn (C. Zhang), ttsui@hhu.edu.cn (T. Sui), crabsaver@163.com (M. Xie).

Ruessink (2005) investigated the nearshore bar response to the nourishment implemented in the trough between the middle and the outer bar in Terschelling, the Netherlands. They found that the bar-trough system would recover to its pre-nourished state after 6–7 years. Pan et al. (2017) analyzed the post-nourishment at the west beach in Qinhuangdao, China, using the EOF method. The nourishing artificial sandbar migrated onshore with its shape becoming asymmetric under low wave energy conditions. Hearin (2014) analyzed historical data to determine the impact of the beach nourishment on morphological modal beach state in the North Reach of Brevard County, Florida. It was noted that the particle size characteristics of filled sands could change the morphological modal beach state.

Field studies mentioned above focused on the long-term evolution of the shoreface nourishment. On a shorter time-scale, a few observations in storm events were also conducted. Elko (2006) presented the detailed sediment transport rate measurements after three hurricanes on Upham beach in west-central Florida. It was found that the profile equilibrium after nourishment could be induced by a storm event, rather than a long-term process. The observations conducted under storms or other extreme weathers are limited by instruments and field conditions, so that bathymetry measurements cannot be carried out frequently. Pietro et al. (2008) developed a method of monitoring the beach nourishment project using a terrestrial LIDAR, which can provide monthly subaerial beach topography. However, the time scale of research mentioned above are much longer than an individual storm wave event scale (e.g., Eichentopf et al., 2020a), which is usually in hours to days. The short-term evolution behaviors of the SAB during short-term erosive events are important for sediment storage and beach erosion/recovery patterns, which still need a detailed analysis.

It is efficient to simulate shoreface nourishment evolution with numerical beach morphodynamic models (e.g., Grunnet et al., 2004; Larson and Hanson, 2015; Luijendijk et al., 2017; van der Werf et al., 2019), all of which paid a special attention to bar shape evolution and energy dissipation on it. Chen and Dodd (2019) related migration and evolution of shoreface nourishment to sediment flux induced by diffusion and divergence terms in their idealized model. They found that the shoreface nourishment migrates onshore or splits into onshore and offshore parts, depending on the breaking intensity. Spielmann et al. (2011) simulated different implementation strategies of shoreface nourishment with a process-based model. Other numerical models have been developed and calibrated for natural sandbar evolution (e.g., van Rijn et al., 2003; Ruessink et al., 2007; Zheng et al., 2014). However, these numerical models are less applicable to simulate the berm evolution due to the lack of swash zone description, so that the berm response to sandbar is difficult to investigate.

Laboratory experiment acts as a well-control method to simulate morphological evolution of the SAB on various time scales. Yuksel and Kobayashi (2020) conducted laboratory experiments to investigate the efficiency of the submerged sill (functioning as SAB) in reducing shore erosion and overtopping. Grasso et al. (2011) observed the shoreface nourishment implemented on a barred profile under the attack of a schematic storm in a wave flume, and analyzed the feeder- and lee-effect of the SAB implemented at different positions. Atkinson and Baldock (2020) investigated the influence of the SAB implementations on shoreline retreat under the sea level rise setting. Guimarães et al. (2021) highlighted the importance of number and positions of the measuring equipment, and demonstrated the inherent constraints in conducting three-dimensional (3D) beach nourishment experiments.

Aforementioned studies showed special interests into the SAB evolution or its function in reducing erosion, but the morphological couplings between the SAB and natural morphology cells are still not very clear. To date, to the best of our knowledge, there are few convincing conclusions about the relationships between berm state and the SAB morphology. Although it is well recognized that the water depth over the SAB is an important design parameter (e.g., Walstra et al., 2011), the effects of other parameters (e.g., bar height, both sides of slopes) require

more considerations. Furthermore, the effect of background beach states (e.g., erosive or accretive) on the SAB evolution still needs to be analyzed. The objective of this study is to analyze the morphological evolution of the SAB and to explore its potential impacts on the beach system under the storm wave condition. The rest part of this paper is organized as follows. Section 2 describes the experimental setup. The main observed results are presented in Section 3. Discussion and conclusions are provided in Sections 4 and 5, respectively.

2. Experimental Setup

2.1. Wave flume and instruments

The wave flume is of 50 m length, 0.5 m width and 1 m height, and was poured with a working water depth of 0.6 m in the horizontal section (Fig. 1). The flume is equipped with a paddle type wave maker, which can generate wave heights up to 0.3 m depending on the working water depth. In the experiment, random waves were generated in JONSWAP spectrum with the peak enhancement factor of 3.3. The beach profile consisted of fine to medium natural sands with density of 2.65 g/cm^3 and median diameter $d_{50} = 0.23 \text{ mm}$, corresponding settling velocity $\omega_s = 3.0 \text{ cm/s}$. The first and last deciles of grain size were $d_5 = 0.16 \text{ mm}$ and $d_{95} = 0.52 \text{ mm}$, respectively. The sorting coefficient between d_{30} and d_{80} was 1.45, indicating the sands were well-sorted. The last 4 m horizontal part was located shoreward of the swash limit and did not show any beach evolution during the experiment. Wave gauges were used to measure the water surface elevations across the beach profile with a sampling frequency of 50 Hz (Xue et al., 2017). The bulk wave analysis is used to calculate root-mean-square wave height (H_{rms}). A bandpass filter is used to remove low-frequency and high-frequency tails with thresholds of half and four times of peak frequency, respectively. The bed elevation is measured with a Trimble scan X configuration scanner with an error less than 1 mm, placed on a tripod platform located at an offshore position. The vertical and horizontal datum are at the SWL and the toe of the profile, respectively.

2.2. Background profiles

To observe the SAB evolution under different background profile settings, two types of background quasi-equilibrium beaches, i.e., the intermediate beach (barred beach) and the reflective beach (berm beach), have been firstly generated from an original 1:20 sloping beach profile under erosive and accretive wave conditions before the construction of the SAB. The overall tendency of a beach (erosive or accretive) under a given wave climate is always determined by the Gourlay number, $\Omega = H_{s0}/\omega_s T_p$ (Gourlay, 1968; Dean, 1977; Dalrymple, 1992). H_{s0} represents the offshore significant wave height, T_p is the peak period. As shown in Table 1, the relatively small wave with H_{s0} of 0.05 m and T_p of 2 s ($\Omega = 0.8$) was used to generate accretive beach with a high remarkable berm. The accretive beach tended to be equilibrium after 14 h wave action (Fig. 2). The berm height was 0.11 m above the SWL and both sides of the slope were steep. The quasi-equilibrium barred beach was formed under a more energetic wave condition ($H_{s0} = 0.16 \text{ m}$; $T_p = 1.6 \text{ s}$; $\Omega = 3.3$) with the duration of 11 h. The outer bar was located from $x = 5 \text{ m}$ to $x = 7 \text{ m}$, with its crest at $x = 6 \text{ m}$. The inner bar was at $x = 10 \text{ m}$.

Scale relations are needed to be clarified in small-scale experimental models (e.g., Hughes, 1993). Comparing with the large-scale experiments (e.g., Baldock et al., 2011; Sanchez-Arcilla and Caceres, 2017; Eichentopf et al., 2020b) and field observations, similar beach profile responses have been observed during accretive and erosive wave conditions, such as the formation of the steep berm and bar-trough feature. It should be acknowledged that the scale effect exists inevitably in local sediment transport at the laboratory scale. Thus, similitude law in terms of the morphological evolution between the modelled beach and prototype beach is achieved in this study, rather than to model a

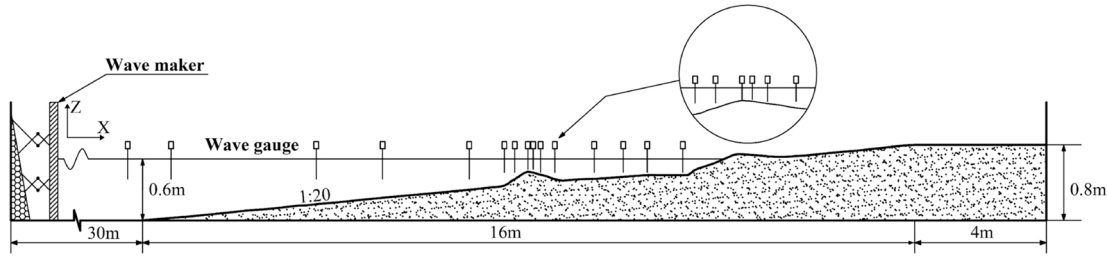


Fig. 1. Sketch of the experimental setup.

Table 1
Summary of wave conditions of two background profiles.

Background Profile	H_{s0} (m)	T_p (s)	$\Omega = H_{s0}/\omega_s T_p$	Profile type	$\zeta = \frac{\tan\beta}{\sqrt{s_0}}$	Surfzone State
A	0.05	2	0.8	Berm	0.56	unsaturated
E	0.16	1.6	3.3	Barred	0.25	saturated

Note: A represents the reflective beach (Accretive berm profile), and E means the intermediate beach (Erosive barred profile). ζ means surf similarity parameter, $\tan\beta$ represents the overall profile slope, s_0 means offshore wave steepness, subscript 0 means offshore wave properties.

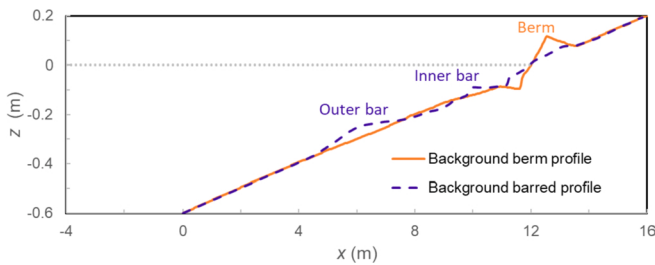


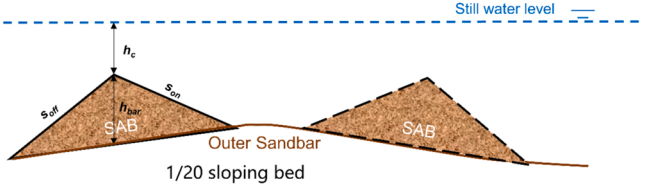
Fig. 2. Background reflective beach (profile A) and intermediate beach (profile E).

particularly real-world beach (e.g., Atkinson et al., 2018; Baldock et al., 2017). To model the beach profile response appropriately, the similarity of $H_{s0} \tan\beta/\omega_s T_p$ proposed by Hattori and Kawamata (1980) was firstly fulfilled. Then the Froude similarity law was used for hydrodynamics. Two types of scale relations can be derived on that basis. The first type is a distorted scale relation with similar sediment size between modelled and prototype scale. According to Atkinson et al. (2018) and Atkinson and Baldock (2020), using similar sand grain size at the laboratory to that in the field would cause that horizontal is larger than vertical scales, and the corresponding prototype beach is milder. For example, taking erosive deep-water peak wave length $L_{p0} = 4.0$ m in this experiment, and considering the peak wave length with relatively large wave heights, were of order 60 m (e.g., the beach near Duck, North Carolina, Ruessink et al., 2003). Thus, the horizontal scale ratio n_L should be chosen about 15, and the vertical scale $n_h = (n_L)^{2/3} = 6$. The overall 1/20 beach in laboratory represents a prototype beach with a gradient approximately 2.5 times smaller. The second type is an undistorted scale relation with geometric similarity ($n_h = n_L$). The grain size ratio should be the same as the geometric ratio. If n_L has been chosen about 16, the grain side on prototype beach is around 0.9 mm.

2.3. Artificial sandbar designs

As shown in Fig. 3, the crest depth h_c is defined as the vertical distance between still water level and the SAB crest. The bar height (h_{bar}) is defined as the maximum vertical variance between initial background profile (A and E) and the profile with the SAB (Alsina et al., 2012;

● Cases on the intermediate beach



● Cases on the reflective beach



Fig. 3. Schematic of SAB designs in this study, scale is not considered. The difference of the solid and dashed lines shows they are not implemented in a test.

Eichentopf et al., 2020b). The shoreline location is the cross-shore location where the still water level intersects the profile (e.g., Baldock et al., 2017; Eichentopf et al., 2020). The shape of the shoreface nourishment is complex on real-world beaches due to the technical limitations of subaqueous sediment filling. Therefore, the geometry shape of the SAB is usually schematized to regular shapes, such as trapezoid (Kuang et al., 2021), the Cosine function shape (Holman et al., 2014, 2016) and the Gaussian function shape (Spielmann et al., 2011). In this study, the triangle SAB was adopted for three aspects. Firstly, the triangle shape can provide specific height and span to recognize the bar as well as its distance from the shoreline (Marinho et al., 2020). Secondly, Jacobsen and Fredsøe (2014) found a more concentrated nourishment can provide a better protection for the beach. A triangle nourishment is narrower in space than that with the trapezoid shape, Cosine function shape and Gaussian function shape. Lastly, real-world nourishment can sometimes exhibit a triangle shape, such as Pan et al. (2017). On the reflective beach, the SAB was implemented within the closure depth. On the intermediate beach, the SAB was implemented on the seaward or shoreward of the outer bar. Similar strategies can be found on the Terschelling beach (Grunnet et al., 2004) and the Egmond beach (van Duin et al., 2004). The ratio of shoreward slope to seaward slope (s_{on}/s_{off}) is designed to be same to that of natural sandbar based on the 1/20 sloping profile. The values of s_{on} and s_{off} are about 4 times larger than that of the natural sandbar to make distinctions from sandbars and to explore its potential impact. The volumes of shoreface nourishments are always in similar magnitude to natural breaker bars (e.g., Walstra et al., 2011; Atkinson and Baldock, 2020; van Duin et al., 2004). As shown in Fig. 3 lower column, the water depth over the SAB crest h_c ranged from 0.07 m to 0.12 m, and s_{off} ranged from 0.19 to 0.27 (cases A1 ~ A4).

The energetic wave condition ($H_{s0} = 0.16$ m; $T_p = 1.6$ s; $\Omega = 3.3$) was also used to represent the storm wave condition imposed on the SAB. It should be noted that the definitions of the storm are highly site-specific

and subjective (Eichentopf et al., 2019). A storm can be defined if the wave height threshold is research, large waves last for a long time (Coco et al., 2014) or remarkable beach profile change occurs (Voudoukas et al., 2012). Therefore, we defined the storm condition following Eichentopf et al. (2020b), in which two storms are defined by Ω of 2.54 and 3.34.

Bed profile measurements were conducted several times during each run, for which the time intervals for all cases are provided in Table 2. Time intervals were not fixed but adjusted according to the time-varying profile evolution rate. Profiles with a smaller h_c tended to evolve more rapidly. Hence Case A4 had a more frequent measurement in the beginning. Since SAB evolution is the focus of this study, a case would be terminated when little SAB change can be observed visually.

3. Results

3.1. Profile evolution

Fig. 4 (a) ~ (d) illustrates morphology evolution under the storm wave condition during cases A1 ~ A4. In general, these four cases present analogous features. Firstly, the SAB migrates onshore with their shapes dissipating gradually. To be specific, the bar height (h_{bar}) decreases and both sides of slopes become mild. Berms are well protected at the beginning, while major erosion occurs only when shapes of SAB are significantly dissipated. Shoreline retreat and decrease in the front slope of the berm are observed at the end of each case. Hence, the lee-effect of the SAB is dynamic and affected by their morphological stability. Moreover, significant overwash deposits are observed on the back slope of the berm at the end of each case when the SAB morphology has been dissipated sufficiently. The SAB in case A1 (Fig. 4a) with an initial h_c of 0.12 m is almost out of function at $t = 40$ min, while A4 (Fig. 4d) with a smaller h_c of 0.07 m keeps protecting the shoreline and berm effectively until $t = 165$ min. Therefore, the initial h_c at the timing of SAB implementation is a key factor for beach protection.

The morphology evolution of cases with the SAB placed on profile E is provided in Fig. 5. Generally, the SAB migrates onshore with its shape decaying. This morphology evolution trend is similar to the cases of berm profile. In the case E1, the SAB is placed on the shoreward slope of the outer bar. The SAB migrates onshore slightly with both s_{on} and s_{off} getting mild. Upper part of the SAB is eroded and both the shoreward and seaward sides of SAB are accreted. The outer bar is well covered and stable, and its trough is filled by the sediment eroded from the SAB. Hence, the outer bar area has been widened. The inner bar migrates onshore, its shoreward slope becomes mild and the seaward slope gets steep. In the case E2, the SAB is placed on the seaward slope of the outer bar. The SAB is gradually eroded, most of eroded sands are carried onshore and deposit on the outer bar. A part of eroded sands is also moved offshore and is accumulated over the toe of the outer bar. Therefore, the shape of the outer bar has been strengthened. The inner bar migrates onshore and a berm above the SWL is gradually developed for both cases. Berm height (H_b) defined as the maximum difference between SWL and studied profile in berm area is increased and its front slope ($\tan b$) becomes steep.

3.2. SAB morphology evolution

Parameters related to SAB morphology and berm geometry are defined in Fig. 6, in which h_c , h_{bar} , s_{on} and s_{off} represent water depth over SAB crest, bar height, shoreward slope and seaward slope, respectively. These four parameters have also been shown in Fig. 3.

Fig. 7 (a) provides bar height changes in the period of profile evolution. The bar height change Δh_{bar} is defined as the variance between instantaneous bar height and initial bar height (h_{bar0}) at the timing of the SAB implementations, i.e., $\Delta h_{bar} = h_{bar} - h_{bar0}$. Bar decay can be clearly observed in these cases. We have normalized the time frame in the experiment to the peak period, the normalized time is hereafter defined as T_N with a unit of 10^3 . When T_N is less than 2.4, the bar height decreases by more than half, indicating the SAB undergoes massive erosion. After that, the erosion rate reduces significantly. For instance, more than 3 cm bar height is eroded during T_N from 0 to 2, however, the remaining bar height of nearly 2 cm decays until $T_N = 12$.

The half-life period T_{half} defined as the time required for the bar height to be decreased by half is a key parameter to reflect the SAB stability. As provided in Fig. 7 (b), T_{half} ranges from 0.72 to 6.09 on profile A, and is from 3.39 to 9.12 on profile E. Although the volume of the SAB on profile E is 4 times larger than those placed on profile A, T_{half} of A4 on profile A is larger than that of E1 on profile E, indicating that T_{half} is not only determined by the filling volume, but also can be affected by other shape parameters. Fig. 7 (c) shows T_{half} versus the ratio of initial crest depth to bar height h_{co}/h_{bar} . It is found that T_{half} decreases with the increase of h_{co}/h_{bar} among cases A1 ~ A4 and E1. This is because the undertow has a great impact on SAB stability. To be specific, wave motion acts as a destructive force to move sands of SAB onshore and dissipate their shapes under stormy wave conditions, while undertow carrying sands from the surf zone to SAB for compensation is a major mechanism of SAB stability. Offshore directed sediment transport rate is determined by the undertow velocity and sediment concentration in water columns, these two factors are all affected by breaking intensity, which is mainly controlled by the h_c over the SAB (Ruessink et al., 2003; van der Westhuysen, 2010; Zhang et al., 2017, 2021a). In this case, A4 has a smallest h_c , which drives most intensive undertow and highest sediment concentration at its shoreward side, thus it has a largest T_{half} . However, case E2 has an even larger T_{half} , though its h_{co}/h_{bar} is not representatively small. Since that the SAB of E2 is located seaward of natural sandbar, where the destructive force is relative weaker. Moreover, the onshore migration of the SAB in case E2 is disturbed by the outer bar.

As presented in Fig. 7 (d), T_{half} increases with the increase of the seaward slope s_{off} . It is related to the reinforced compensative offshore sediment transport induced by steep seaward slope. Recent studies show sediment concentration is essentially affected by wave breaking types, as plunging breakers can stir more sands into water column compared with spilling breakers (e.g., Van Der et al., 2017; van der Zanden et al., 2016; van der Zanden, and van der A, D. A., Cáceres, I., Hurther, D., McLelland, S. J., Ribberink, J. S., and O'Donoghue, T., 2018). According to the surf similarity parameter proposed by Battjes (1974), it can be inferred that more individuals in a wave train are likely to break in the plunging type over the steeper seaward slope. In Fig. 7 (e), there is no obvious relations found between T_{half} and s_{on} .

Fig. 8 provides both slopes of the SAB, the seaward slope is defined as positive and vice versa. Generally, both slopes decrease with time. Major changes in seaward slope occurs in the beginning, e.g., seaward slope of case A3 decreases from 0.2 to 0.08 during T_N from 0 to 1.5. After that, all cases show a similar behavior that both slopes evolve towards a relative stable state. The stable seaward slope is steeper than shoreward slope in magnitude. Two exponential curves are used to describe the SAB slope response to the storm wave condition with R^2 of 0.9 and 0.7 for offshore and shoreward slope, respectively.

Table 2
SAB designs and implementations.

Case ID	Background profile	h_c (m)	s_{off}	Bed profile measuring moments (min)
A1	A	0.12	0.24	$t = 0; 7.5; 15; 40$
A2	A	0.11	0.19	$t = 0; 7.5; 15; 40; 65$
A3	A	0.09	0.25	$t = 0; 7.5; 15; 47.5; 97.5$
A4	A	0.07	0.27	$t = 0; 5; 15; 90; 165$
E1	E	0.13	0.23	$t = 0; 25; 100; 162.5$
E2	E	0.22	0.25	$t = 0; 45; 307.5$

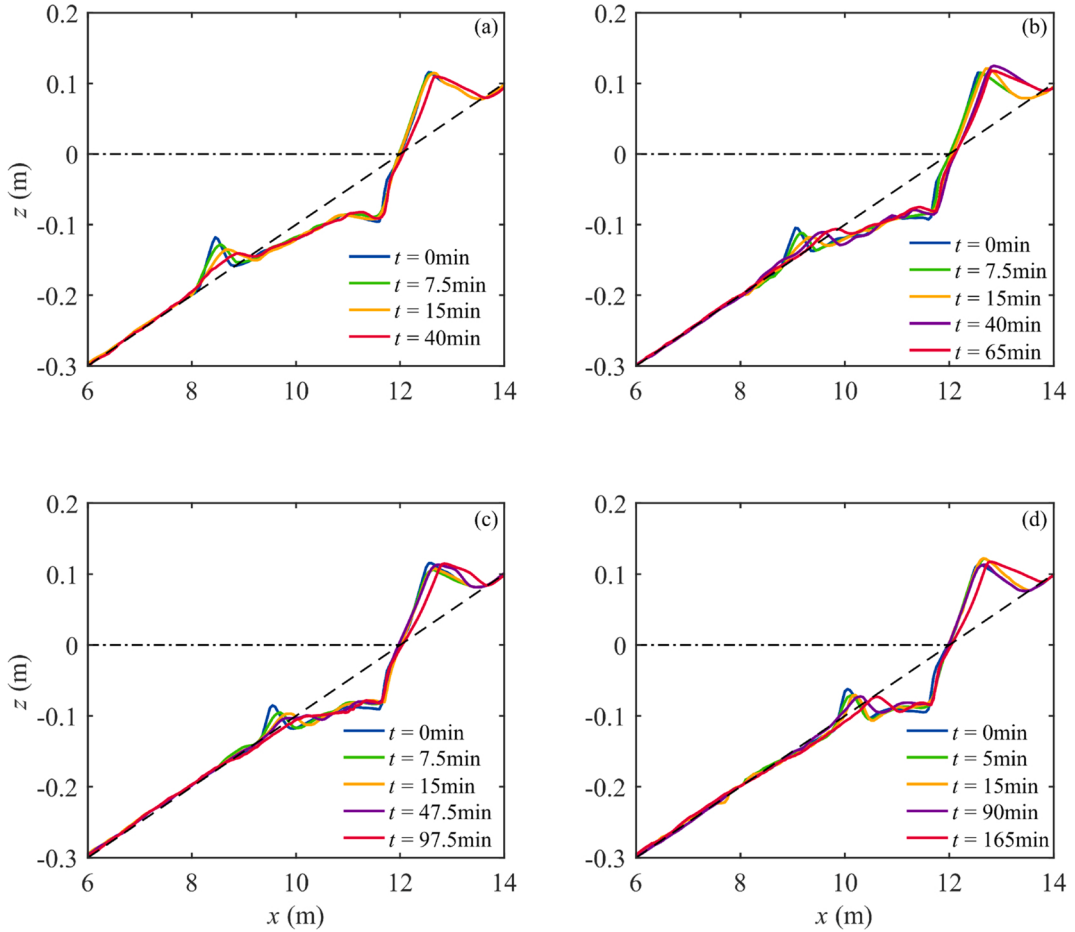


Fig. 4. Beach profile evolution for cases A1 (a), A2 (b), A3 (c) and A4 (d). Dash-dotted line represents still water level and dashed line indicates initial sloping profile.

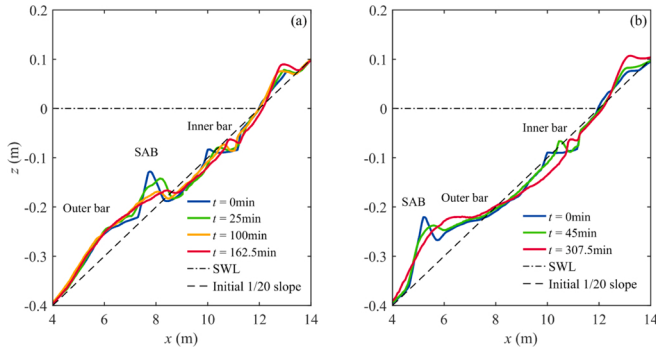


Fig. 5. Profile evolution for cases E1 (a) and E2 (b). Dash-dotted line represents still water level and dashed line indicates initial sloping profile.

3.3. Berm responses

As defined in Fig. 6, The berm front slope ($\tan b$) is the average of the flat slope above the still water level. The erosion pattern of berm is like the rollover of islands on reef flat (Masselink et al., 2020), which involves sediment transport from the front of berm to the top and back of the berm via overtopping and overwash processes. Therefore, the berm rollover ($\tan \theta$) is defined as the slope between the positive direction of x axis and the line connecting berm highest position to the initial shoreline location (i.e., at the timing of the SAB implementation). Berm responses are specifically investigated on the profile A, which has a remarkable berm before nourishment. In this work, $\tan b$ and $\tan \theta$ are referred to as indicators for berm responses.

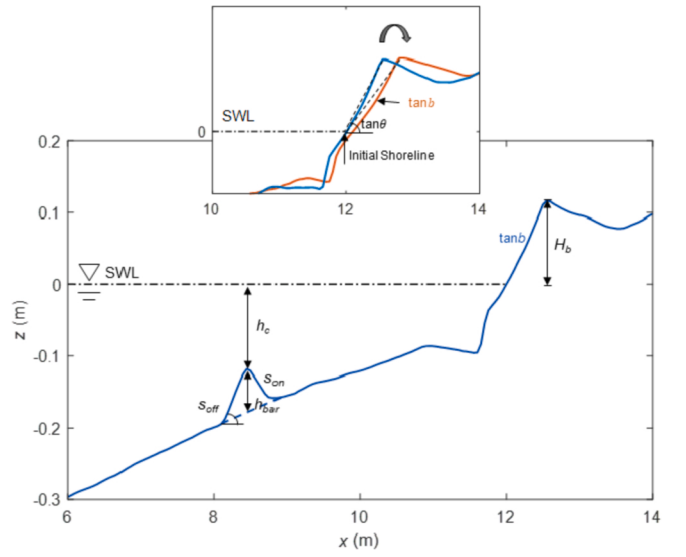


Fig. 6. Definitions of parameters to describe the morphology of SAB and berm.

As provided in Fig. 9 (a), normalized berm front slope ($\tan b / \tan b_0$) is plotted against time for each case on profile A. It is revealed that $\tan b / \tan b_0$ generally decreases with storm wave duration, and is in line with the traditional findings of relationships between the beach slope and wave conditions (e.g., Wright et al., 1985; Short and Hesp, 1982; Jackson and Short, 2020). However, an obvious increasing trend occurs

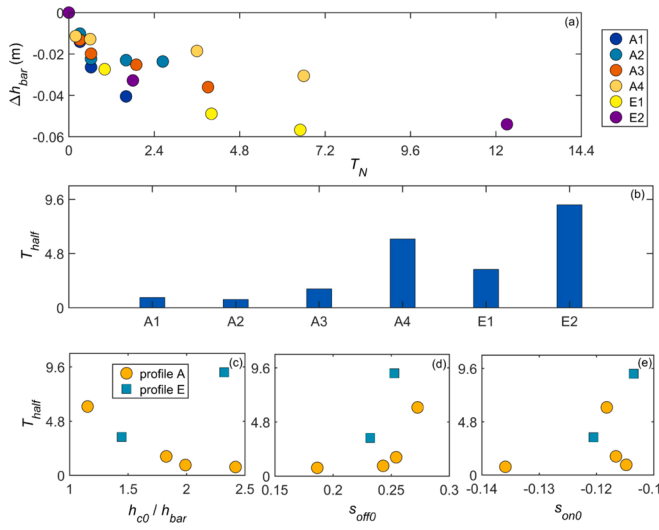


Fig. 7. Bar height change versus time (a), half-life period of SAB for each case (b), half lifetime versus initial crest depth (c), initial seaward slope (d) and initial shoreward slope (e) of SAB. The subscript 0 indicates the initial SAB parameter.

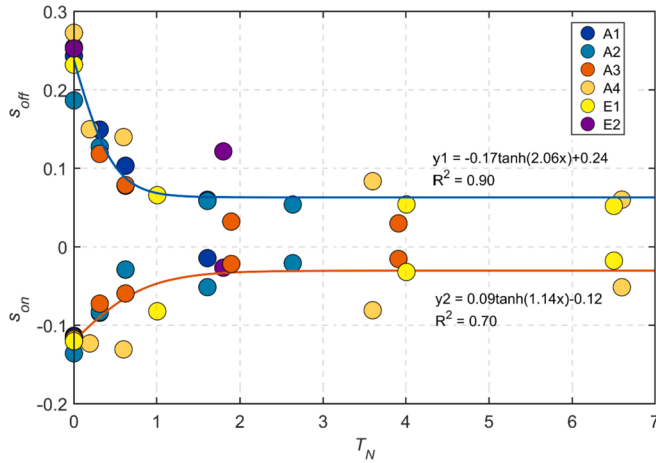


Fig. 8. Time variations of the shoreward and seaward slopes of the SAB.

before decrease during T_N from 0 to 0.6, indicated by $\tan b/\tan b_0 > 1$. This is a morphological hysteresis of berm response to erosive wave impacts, and it is due to the time-dependent lee effect of the SAB, i.e., the SAB have strong capabilities to trigger breakers in the beginning so that the wave energy becomes weak when propagating to the shoreline. This kind of incipient deposition can also be observed from Fig. 4 (a), (c) and (d) visually. The accretive intensity is affected by h_{c0} , case with a smaller h_{c0} is more likely to have an intense initial deposition (e.g., case A4 with a smallest h_{c0} has the longest and most intense deposition). After $T_N = 0.6$, erosion occurs, indicating $\tan b/\tan b_0 < 1$. The erosion rate is also dependent on h_{c0} , case with a smaller h_{c0} is more likely to have a smaller erosion rate.

Berm rollover acts as an indicator of berm overall behavior. Fig. 9 (b) provides normalized rollover ($\tan\theta/\tan\theta_0$) versus time. In the beginning, berm rolls to landward in a higher rate in each case. After $T_N = 3$, the evolution of $\tan\theta/\tan\theta_0$ turns to be equilibrium of approximately 0.72. An exponential relation is employed to capture this trend, with $R^2 = 0.88$. The higher landward rollover rate indicates the mismatching between initial accretive profile and the prevailing storm wave condition. Under the given wave condition for sufficiently long time, the berm turns to be equilibrium, which shows that rollover can reflect berm

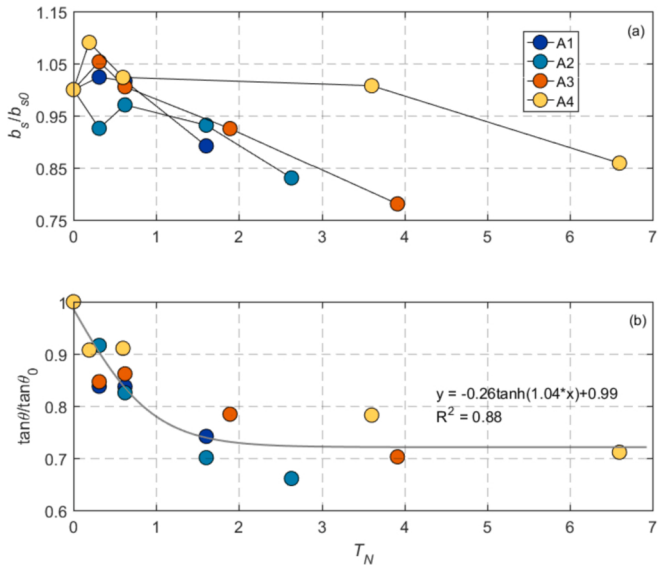


Fig. 9. Time variations of normalized berm front slope (a) and rollover (b).

response in a relatively longer time-scale in the present experiments.

4. Discussion

4.1. Influence of SAB on sediment transport

Some of the previous studies argued that smaller scales of morphology perturbations are mechanisms for larger coastal evolution (e.g., Winter et al., 2008; Murray et al., 2009; Wengrove, 2018). Onshore migration of the SAB or natural intertidal sandbars act as ‘sands reservoir’ providing significant sediment resources to feed upper beach parts (Price and Ruessink, 2011; Ruggiero et al., 2016). Resolving the sediment transport of the SAB is a complicated task, since the mechanisms of sediment pick-up rate are not very clear under this circumstance (Chen et al., 2018; Chen et al., 2021; Sui et al., 2021). The net cross-shore sediment transport rate per unit width, q_t , is calculated with sediment volume conservation equation:

$$q_t(x_i) = q_t(x_{i-1}) - (1-p) \int_{x_{i-1}}^{x_i} \frac{\Delta z}{\Delta t} dx \quad (1)$$

in which, $q_t(x_i)$ represents the net total (bedload and suspended load) sediment transport rate at position x_i . q_t is positive for onshore sediment transport and negative for offshore sediment transport. Δz is the changes of bed elevation within time interval Δt from x_{i-1} to x_i . p is sands porosity taken as 0.4. Eq. (1) is integrated from seaward limits to shoreward limits of active profile located at closure depth and overwash limits, respectively. At shoreward or seaward boundary, closure errors could occur due to profile alongshore variance or sediment compaction. A correction method is introduced to ensure zero sediment transport across the boundary, which distributes the sediment volumetric error uniformly across the active profile, following Baldock et al. (2011); Alsina et al. (2012); Eichendorf et al. (2020b) and Atkinson and Baldock (2020).

Net sediment transport rate on background profile A and E are provided in Fig. 10. On profile A, onshore sediment transport dominates and the maximum sediment transport rate occurs at $x = 12$ m, corresponding to the formation of the berm. On profile E, offshore sediment transport dominates and its maximum locates at 0.5 m shoreward of the outer bar. Onshore sediment transport also occurs due to the overwash deposits under the storm wave condition. The sediment transport modes and directions on profile A and E are typical patterns under accretive and erosive wave conditions, which have been stated in previous studies (e.

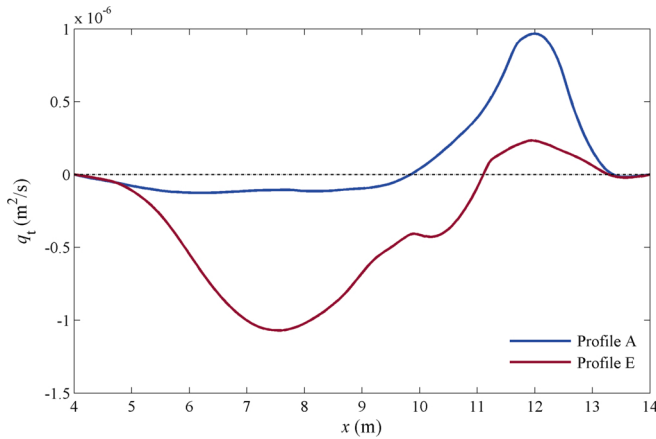


Fig. 10. Sediment transport on background profile A and E.

g., Ruessink et al., 2007; Zheng et al., 2014).

After the implementation of SAB on profile A, SAB welds onshore and is served as a sediment feeding source for inner surf zone. Fig. 11 shows the profile evolution and net sediment transport for cases A2 and A4. Although the wave duration differs (65 min for A2 and 165 min for A4), their sediment transport patterns are similar. Due to the impact of the storm wave condition, sediment transport rate in major part of shoreface is offshore directed. While the sediment transport direction has been altered to onshore at the implementation position of the SAB, indicating that the SAB can change local sediment transport modes and beach state. Comparing Fig. 11 (c) and (d), it is noted that shoreward placement of SAB can reduce net offshore sediment transport rate in the inner surf zone.

Fig. 12 illustrates net sediment transport patterns for cases E1 and E2. It should be stated that wave durations for these two cases are different (163 min for E1 and 308 min for E2), but it does not affect the analysis for sediment transport modes and directions. As provided in Fig. 12 (a) and (c), maximum offshore sediment transport occurs at the trough of the outer bar. However, it has been switched to onshore direction after the implementation of the SAB. Hence, it can be inferred that implementation of the SAB on natural bar trough can weak the offshore sediment transport to prevent trough erosion. Shoreward of the SAB, two peaks of onshore sediment transport occur. One of the peaks is located at $x = 10.5$ m accounting for the onshore migration of inner bar. The other peak occurs at $x = 12.5$ m promoting the formation of berm. As shown in Fig. 12 (d), the maximum offshore sediment transport occurs at the trough of the outer bar, and the SAB changes sediment transport direction locally at seaward of the outer bar. Comparing Fig. 12 (c) and (d), the SAB implemented on the trough of the outer bar is more efficient in reducing offshore sediment transport and beach

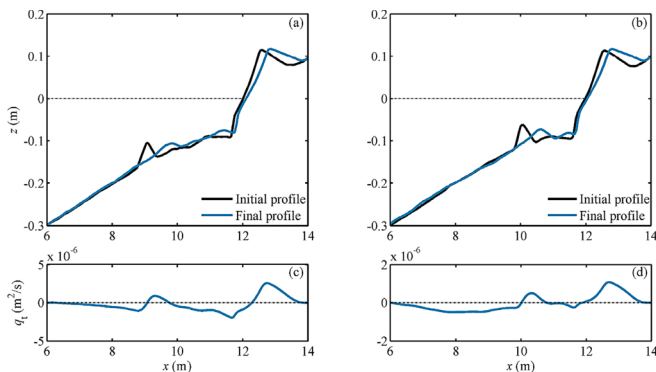


Fig. 11. Profile evolution and net sediment transport rate for case A2 (left panel) and case A4 (right panel).

erosion than that placed on the seaward of the outer bar. However, the position of accretion-erosion balance point (located at $x = 10$ m would not be moved whether the SAB is placed on the shoreward or seaward of the outer bar. These two implementation strategies have been used in shoreface nourishment projects at Terschelling beach (Grunnet and Ruessink, 2005) and Egmond beach (van Duin et al., 2004), in the Netherlands.

4.2. Morphological coupling between SAB and berm

The morphological connections and sediment budgets between the lower shoreface and upper beach have attracted lots of attention. Aagaard (2014) estimated the sediment transport in the lower shoreface with field datasets. Marinho et al. (2020) simulated the sediment budget between bars and berms with a semi-empirical numerical model. Predictive and descriptive parameters are widely used to predict or describe beach state (Battjes, 1974; Dean, 1977; Hatori and Kawamata, 1980; Wright and Short, 1984). However, these empirical parameters could not reflect the influence of artificial structures on the beach state. As provided in Table 1, surf similarity parameter ζ equals 0.25 for offshore wave height 0.16 m, peak period 1.6 s and overall slope of 1/20, indicating the surfzone is saturated (Baldock et al., 1998) and beach state is erosive. However, the beach state has been altered locally from erosion to accretion after the implementation of the SAB. Therefore, following Battjes (1974), an empirical predictive parameter ζ_A is proposed taking the SAB shape parameters into consideration:

$$\zeta_A = \left(\frac{s_{off}}{\sqrt{H_0/L_0}} \right) / \left(\frac{h_c}{h_c + h_{bar}} \right) \quad (2)$$

where the first term in numerator is a surf similarity parameter based on the seaward slope of the SAB. This term with a larger magnitude indicates a higher possibility of occurrence of plunging breakers, i.e., onshore sediment transport. The term in denominator represents relative bar height. A smaller magnitude of this term means a smaller h_c or larger h_{bar} , indicating a better lee-effect so that the berm is more likely to be accretive (or not to be eroded). When there is no SAB, s_{off} in Eq. 2 equals original beach slope and h_{bar} equals 0, so that ζ_A reduces to the classic surf similarity parameter of Battjes (1974).

To adapt to incoming wave conditions and subaqueous beach profile evolution, the berm shape changes accordingly mainly in three ways (i.e., $\tan b$, H_b and $\tan \theta$ changes). Hence, the berm response parameter Ψ should be the function of $\tan b/\tan b_0$, H_b/H_{b0} and $\tan \theta/\tan \theta_0$:

$$\Psi = f\left(\frac{\tan b}{\tan b_0}, \frac{\tan \theta}{\tan \theta_0}, \frac{H_b}{H_{b0}}\right) \quad (3)$$

where the physical meanings of $\tan b/\tan b_0$, H_b/H_{b0} and $\tan \theta/\tan \theta_0$ are relative changes of the berm foreshore slope, the berm height and the berm rollover compared with those at the timing of shoreface nourishment implementation, respectively. Their values larger than 1 means berm foreshore slope becomes steeper, berm height gets larger and berm seaward rollover, indicating berm state is accretive, and vice versa.

The above Eq. 3 involves a functional dependence on three variables, however, whether the changes of these three variables are dependent on SAB morphology remains unknown. To scale these potential dependences, we plot H_b/H_{b0} , $\tan b/\tan b_0$ and $\tan \theta/\tan \theta_0$ versus ζ_A in Fig. 13. It can be found that both $\tan b/\tan b_0$ and $\tan \theta/\tan \theta_0$ are well captured with a hyperbolic tangent function of ζ_A well R^2 of 0.65 and 0.83, respectively. While the relationship between H_b/H_{b0} and ζ_A is not obvious, indicating that the berm height change is less sensitive to SAB morphology than other two variables and it thus has been discarded in the analysis of SAB-berm coupling. It is therefore assumed that the berm response parameter Ψ is linear combination of $\tan b/\tan b_0$ and $\tan \theta/\tan \theta_0$. To ensure $\Psi = 1$, when $\tan b/\tan b_0 = 1$ and $\tan \theta/\tan \theta_0 = 1$, Ψ can be written as,

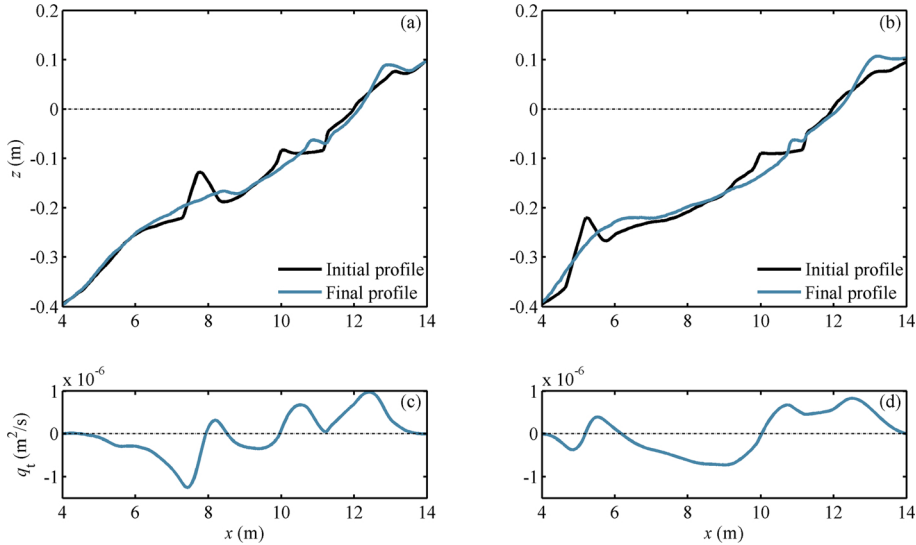


Fig. 12. Profile evolution and net sediment transport rate for case E1 (left panel) and case E2 (right panel).

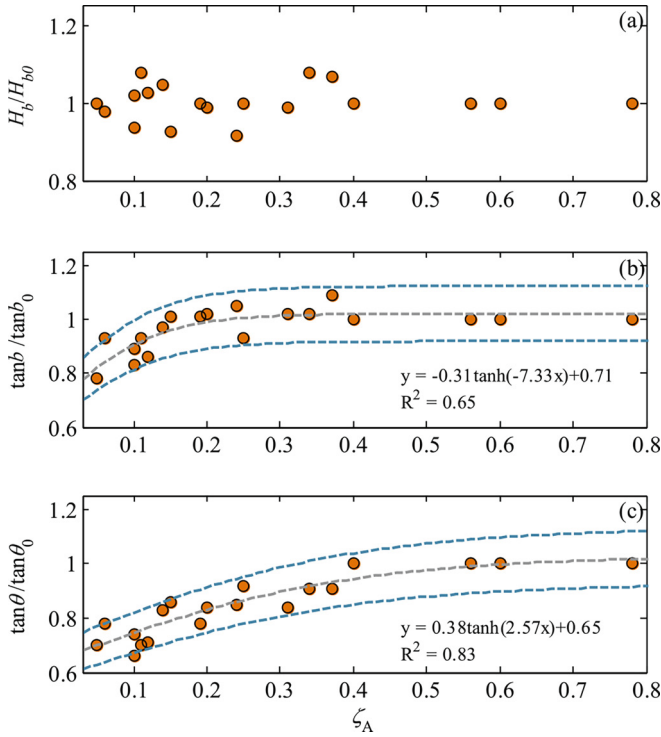


Fig. 13. Graphical dependences on ζ_A for (a) H_b/H_{b0} , (b) $\tan b/\tan b_0$ and (c) $\tan \theta/\tan \theta_0$. Orange circles are measurements, grey dashed line is fitted curve and blue dashed lines are 10% error lines. (For interpretation of the references to colour in this figure legend, the reader is referred to the web version of this article.)

$$\Psi = \alpha \frac{\tan b}{\tan b_0} + (1 - \alpha) \frac{\tan \theta}{\tan \theta_0} \quad (4)$$

in which, α is a tunable constant ranging from 0 to 1. Since that $\tan b/\tan b_0$ and $\tan \theta/\tan \theta_0$ are the hyperbolic tangent functions of ζ_A , Ψ is also a hyperbolic tangent function of ζ_A and can be written as:

$$\Psi = A \tanh(B\zeta_A) + C \quad (5)$$

where A, B, and C are all constants that are dependent on α , their magnitudes and corresponding α and correlation coefficients are shown

in [Table 3](#). The measured and calculated relationships between Ψ and ζ_A with $\alpha = 0.1, 0.5$ and 0.9 are shown in [Fig. 14](#).

Based on this relationship, it is noted Ψ increases with the increasing of ζ_A , and gradually tends to be stable. The morphological coupling reveals the berm responses is controlled by the SAB morphology. The berm undergoes less erosion with the protection of SAB which has a smaller h_c and steeper s_{off} under the erosive wave condition. When Ψ is larger than 1, the berm is accretive compared with the state before the nourishment, indicating there is a morphological hysteresis of berm response to erosive wave impacts, when the morphology of the SAB is remarkable. Meanwhile, the SAB with a steep s_{off} and a smaller h_c efficiently dissipates the incident wave energy. When the SAB is decayed with a milder s_{off} and larger h_c (i.e., with a small ζ_A), the morphological hysteresis is vanished and the berm starts to be eroded with a small Ψ .

4.3. Numerical modelling

In order to examine the capability of existing numerical models for describing the onshore migration of the SAB under the storm condition, the CROSPE model developed by [Zheng et al. \(2014\)](#) is tested in this study. The model is calibrated to provide more details on hydrodynamics and sediment transport patterns for in-depth analysis of underpinning mechanisms. The CROSPE model predicts depth- and phase-resolving variation of flow velocity, suspended sediment concentration and sediment transport rate, and takes the effects of nonlinear wave-undertow interaction on sediment transport into consideration. It has been used to model barred equilibrium beach profile ([Li et al., 2021a](#)) and onshore migration of the shoreface nourishment under mild wave conditions ([Li et al., 2021b](#)). To avoid excessive erosion in front of the shoreline, an empirical correction is added to the original model to modify sediment transport rate from the shoreward boundary of surf zone to the runup limit, following [Roelvink and Costas \(2017\)](#) and [Rafati et al. \(2021\)](#).

In the calculation domain, a uniform mesh is used horizontally with a grid spacing of 0.05 m. In the vertical direction, 100 grid cells are set with the space increasing logarithmically from bed to wave trough. The

Table 3
Constants in Eq. 5 and corresponding α and correlation coefficients.

α	A	B	C	R^2
0.1	0.36	2.74	0.66	0.84
0.5	0.31	4.23	0.70	0.82
0.9	-0.31	-6.65	0.71	0.70

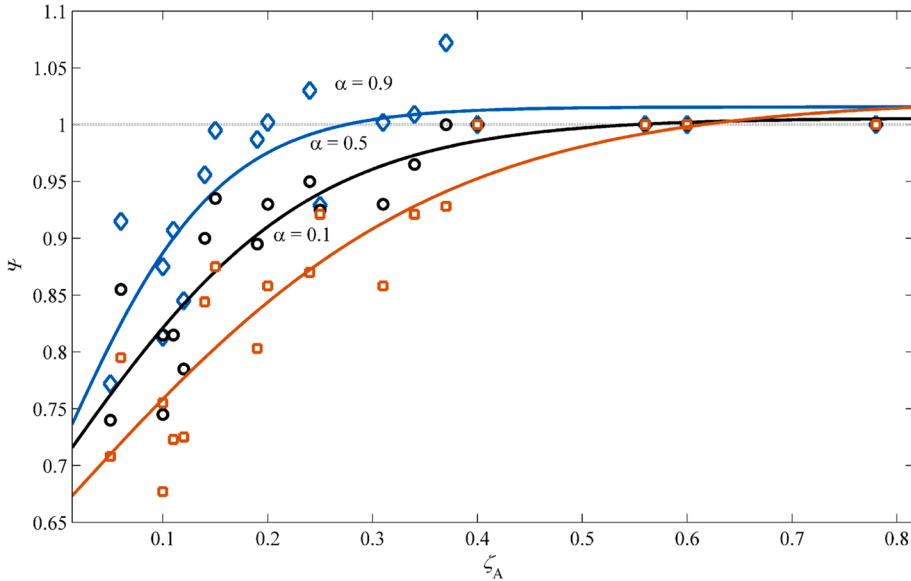


Fig. 14. Quantitative relationship between the SAB morphology and berm morphology. Circles, diamonds and squares are measurements and solid lines are fitted curves.

model includes four tunable parameters: the roller slope, the turbulent scaling coefficient, the phase shift angle and the Prandtl/Schmidt number. Case A1 and E1 are selected to represent the regime of the SAB implemented on the reflective beach and intermediate beach. The calibrated values for both cases are 0.15, 0.055, 15 degrees and 1.

Comparison of root-mean square wave height H_{rms} in case E1 is provided in Fig. 15(a), the incipient breaking point occurs on the outer bar at approximately $x = 6$ m. Waves begin to shoal with wave height increasing at the seaward toe of SAB, and then break over the crest of SAB. More shoreward, a remarkable wave breaking point over the inner bar. The CROSPE model simulates wave propagation, shoaling and breaking using a period-averaged wave energy conservation equation (Zheng et al., 2014), in which, the wave breaking energy dissipation is estimated with the method of Janssen and Battjes (2007). The model is capable of reproducing H_{rms} both in magnitude and trend. The predicted and measured horizontal gradient of sediment transport rate dq/dx are

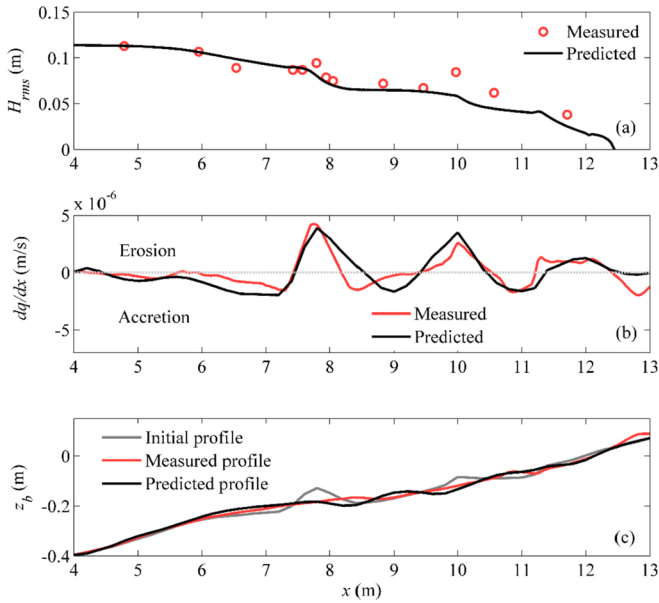


Fig. 15. Comparison of wave height (a), horizontal gradient of sediment transport rate (b) and beach profile evolution (c) in case E1.

compared in Fig. 15(b). A local positive dq/dx represents erosion and vice versa. The predicted dq/dx corresponds well with the measured data inverted from the beach profile change. Comparison of beach profile evolution is provided in Fig. 15(c), the model correctly reproduced the measured beach profile at the end of this test.

Beach profile evolution is a result of imbalance between bedload transport and suspended transport (Li et al., 2021a). Based on the model results, sediment transport patterns are revealed. As provided in Fig. 16 (a), the negative period-averaged and depth-integrated bedload transport rate q_b occurs on the seaward slope of SAB from $x = 6.8$ m to 7.9 m, on the seaward slope of inner bar from $x = 9.0$ m to 9.8 m, and on the beach scarp from $x = 11.2$ m to 11.8 m, since the steep slope favors

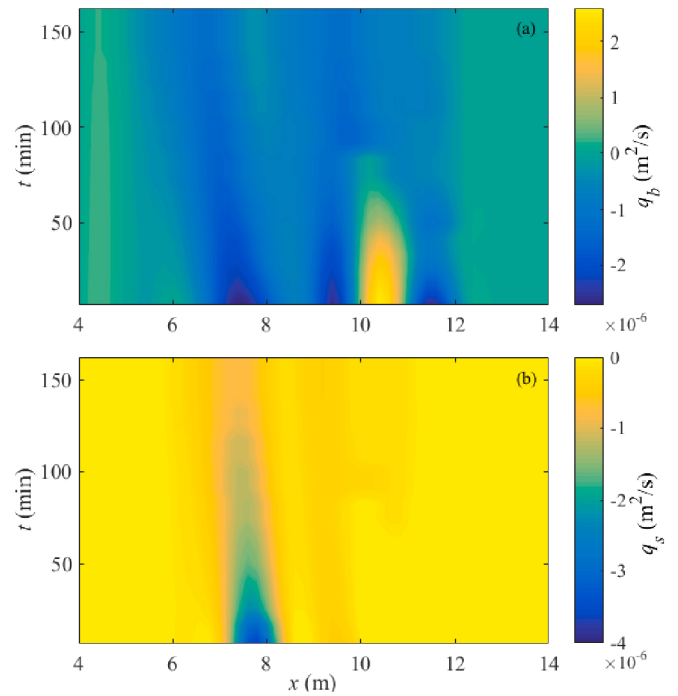


Fig. 16. Spatio-temporal evolution of bedload transport rate (a) and suspended sediment transport rate (b) for case E1.

offshore bedload transport. Maximum onshore q_b occurs in the inner surf zone from $x = 10.2$ m to $x = 10.8$ m due to large wave asymmetry in this area (Li et al., 2021b). As shown in Fig. 16(b), suspended sediment transport rate q_s is offshore directed. As mentioned above, the onshore-directed q_s occurring from $x = 8.2$ m to 8.7 m is not considered in the CROSPSE model. There are two peaks located on the trough of the outer bar from $x = 7.2$ m to 8.4 m, and on the shoreward side of SAB from $x = 9.2$ m to 9.8 m. Both magnitudes of each sediment transport component decrease with time, indicating the beach profile tends to be quasi-equilibrium.

Based on the model results, high spatio-temporal dataset of undertow velocity can be obtained. The spatio-temporal evolution of the net depth-integrated undertow velocity U is provided in Fig. 17. The maximum U occurs on SAB, which is consistent with the Fig. 17(b). The magnitude of U on SAB decreases with time when SAB is gradually dissipated. The similarity between U and q_s shown in Fig. 16(b) indicates that the decrease of undertow velocity is a major cause of the decay of suspended sediment transport rate.

Fig. 18 shows the depth-varying undertow velocity profile from bottom to wave trough level on the initial profile. Seaward of SAB, it can be found that the undertow profile tends to be uniform vertically and the overall magnitude of undertow velocity is smaller than that on SAB or in the inner surf zone. On SAB area, the overall undertow velocity magnitude is largest compared with other areas. The maximum velocity occurs at the bottom, and the undertow velocity decreases with water depth. In the gap-area between SAB and shoreline, onshore undertow velocity occurs near the wave trough level. The pattern of undertow velocity distribution is similar to the observations in CROSSTEX large scale experiment (Scott et al., 2004).

As shown in Fig. 19(a), for Case A1, the model predicts the wave height well both in the trend and magnitude, except underestimates it on the crest of the SAB. However, the model fails to reproduce onshore migration of the SAB in Fig. 19(c). The model result exhibits an offshore migration pattern, it underestimates onshore sediment transport gradient from $x = 8.5$ m to $x = 9$ m in Fig. 19(b). The correspondence between the model results and experimental measurements will not be obviously improved by further tuning model parameters. This is because the CROSPSE model cannot account for the phase coupling between the moment of injection of plunging jets into bottom and the timing of wave crest. Specifically, based on the video recording during each test, it was visually observed that most waves break over the SAB in the plunging type. The transition of spilling breaker to plunging breaker due to the steepened bottom slope was also reported by Zhang et al. (2017). The plunging breaker favors onshore sediment transport because wave breaking turbulent energy injects to bottom in phase of wave crest (Aagaard et al., 2018). Therefore, it can be inferred that the net onshore sediment transport under the storm wave condition is attributed by the phase coupling between the arrival of the turbulent energy and wave crest. The CROSPSE do not take this effect into account in the current version, nor do the most existing numerical models to the best of the

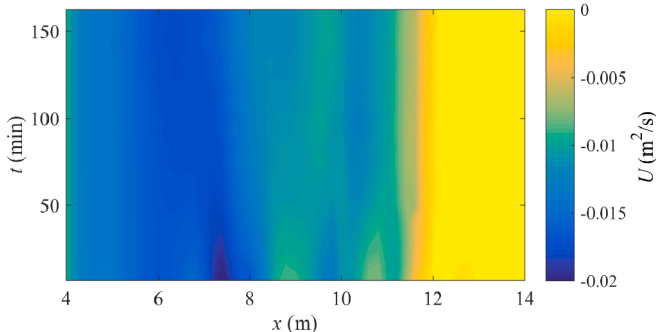


Fig. 17. Spatio-temporal evolution of net depth-integrated undertow velocity for case E1.

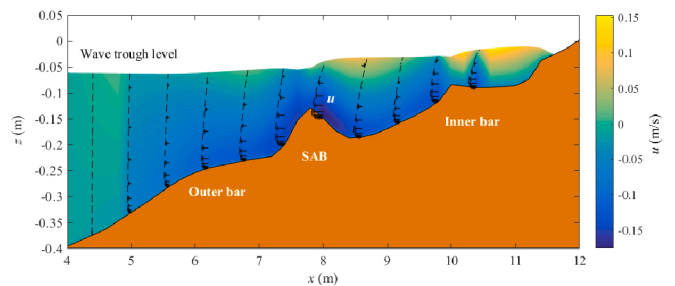


Fig. 18. Depth-varying undertow velocity profile on the initial profile for case E1.

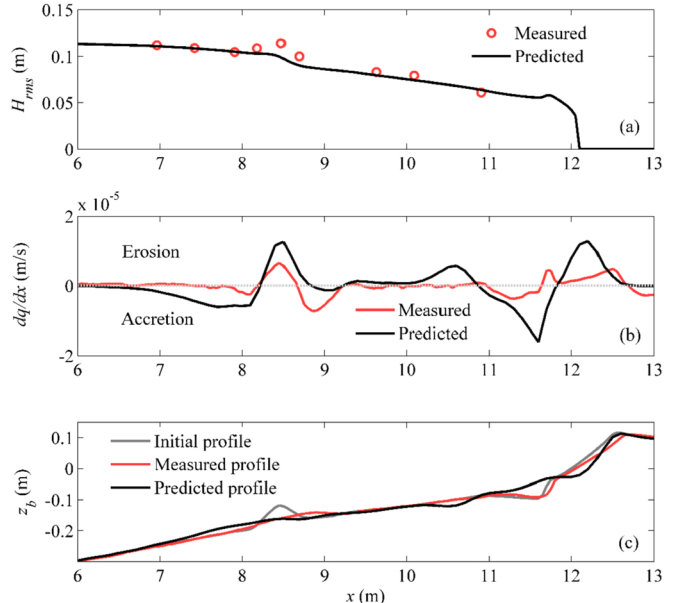


Fig. 19. Comparison of wave height (a), horizontal gradient of sediment transport rate (b) and beach profile evolution (c) in case A1.

authors' knowledge.

Under storm wave conditions, the SAB affects both the dynamic conditions and responses of each component in SAB-gap area-berm system mainly by changing the wave energy dissipation distribution on the whole beach profile. In order to quantify the ability of the SAB to reduce wave energy, the wave energy dissipation (D_b) is modelled with the measured beach profile in cases A1 ~ A4, and the energy dissipation rate K_B is defined as:

$$K_B = \frac{\int_{x_i}^{x_t} D_b dx}{F_{w0}} \quad (6)$$

in which, x_i and x_t represent the horizontal position of incident side and transmission size of the SAB, respectively. As the time goes on, the transitions between the SAB and undisturbed profile become smooth, making the incident and transmission sides difficult to identify. Onshore and offshore spreading of sediments from the SAB increases the cross-shore span of the SAB, leading to the overestimation of Eq. (5). Therefore, we set the cross-shore span fixed as its initial value, and find the position of local maximum elevation as the crest of the SAB x_c . Then $x_i = x_c - 0.5\text{span}$, and $x_t = x_c + 0.5\text{span}$. Although Zhang et al. (2021b) defined the seaward slope toe with the distance of a wave length prior to the maximum wave dissipation over the underwater structure, this algorithm is not applicable to this study since the span of the SAB is smaller than the incident mean wave length in most cases (not shown here). F_{w0} means wave energy flux estimated with wave peak period

using linear wave theory at the seaward edge of the experimental section. In addition, the wave height transmission coefficient K_H is calculated with the experimental results directly (van der Meer et al., 2005):

$$K_H = \frac{H_t}{H_i} \quad (7)$$

in which, subscripts t and i indicate the position of the wave gauge located on the transmission side and incident side of the SAB respectively.

As can be seen in Fig. 20(a) and (b), no obvious relationship is found between K_H and ζ_A , or between K_H and Ψ . In Fig. 20(c), K_B is found increasing with ζ_A , corresponding to that a SAB has a steep seaward slope and a small crest water depth can trigger more wave dissipation. The trend can be captured with a power function with R^2 of 0.57. As shown in Fig. 20(d), Ψ increases with the increase of K_B , indicating the berm can experience less erosion when the SAB can trigger more wave dissipation. The trend is also captured with a power function with R^2 of 0.55. These two trends explain the morphological coupling between Ψ and ζ_A from the perspective of the wave energy dissipation, and provide direct evidence that the SAB protects the rear beach berm by weakening wave energy, i.e., the lee effect.

4.4. Limitations and future works

The SAB migrates onshore with its bar shape dissipating, providing a paradigm shift away from the traditional understanding that the net subaqueous sediment transport is always offshore directed under storm wave conditions. The onshore migration of the SAB is remarkable when its crest water depth is small. Similar observation was conducted in Grasso et al. (2011) in a wave flume with a similar size to that used in this study, the shoreface nourishment implemented on the crest of the breaker bar migrated onshore during the rising stage of the storm in their Fig. 5, case N2. Onshore migration of the shoreface nourishment in the first year after the implementation was also found at four Dutch coasts, i.e., Delfland, Rijnland, North Holland and Terschelling coast in 1997, 2002, 1999 and 1993, respectively (Huisman et al., 2019).

However, the observed trends of the SAB morphology and the relationship between the SAB and the berm in this study cannot be extrapolated to other SAB-beach configurations at real-world coasts without detailed comparisons of external dynamic conditions and morphological surroundings. In the prototype settings, the behavior of the SAB is more complicated since wave and tide conditions from the sea boundary changes and the morphology of the shoreface nourishment is in constant motions. Huisman et al. (2019) found the alongshore current is a main driving force to move the shoreface nourishment, and about 35% (volumetric) of the shoreface nourishment was diffused after three years. Similar observations are reported by Smith et al. (2017), who

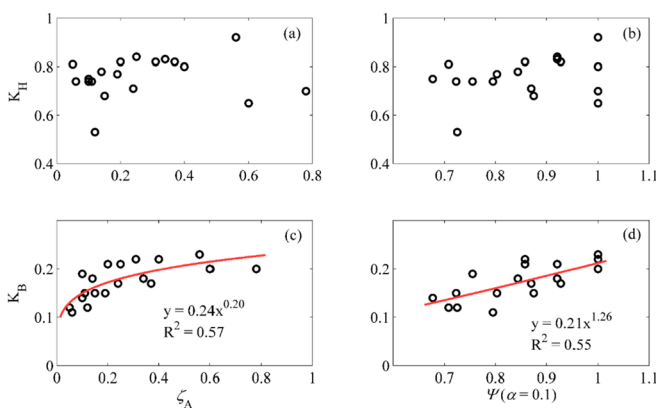


Fig. 20. Relationships between K_H and ζ_A (a), K_H and Ψ (b), K_B and ζ_A (c), K_B and Ψ (d).

found the sediment of shoreface nourishment was mainly dispersed and transported downdrift by longshore current and the morphology of the shoreface nourishment was almost dissipated in the larger scale wave basin. Compared with real-world beaches, the morphology of the SAB in this study is more stable. This is mainly because the inherent limitation of the wave flume experiment that cannot take the alongshore current into consideration. In addition, the vertical change of the SAB is limited in the laboratory settings due to the fixed mean water level. The effect of tide modulation can play an important role in responses of bar crest elevation for the SAB (Nielsen and Shimamoto, 2015). The performance of the SAB is connected to its three-dimensional shape and size, including crest water depth, seaward/shoreward slopes, cross-shore/longshore span, height and orientation. The seaward slope and crest are more predominated on wave-dominated sandy beaches because they change wave breaking type and wave breaking dissipation essentially (Battjes, 1974; Ruessink et al., 2003; Zhang et al., 2021a). The grain size of sediment resource for the SAB is another important factor. Sediment resources are usually dredged from navigation waterways, and hold different grain size from the pre-nourished beaches (McFall et al., 2021). The SAB with a coarse grain size is more stable than that with a fine grain size. Implementation of the SAB has a nonnegligible effect on local sediment compaction structure. Roman-Sierra et al. (2014) found the sand porosities ranges from 0.26 to 0.43 after implementation of the beach nourishment, instead of the fixed value of 0.4. Therefore, sediment samples are needed from offshore, SAB to berm for the estimation of sediment transport and morphology evolution.

Above all, the findings are achieved from an idealized triangle SAB with a steep seaward slope that is four time larger than the local slope of undisturbed bottom. It provides a possibility to use such type of shoreface nourishments to prevent severe erosion under storm conditions. Moreover, the datasets measured in the experiment are useful for further calibration of numerical models to include more physical details. Future works are mainly in the following two aspects. On the one hand, a comprehensive 3D integrated numerical model can serve as a useful tool to reveal the morphological responses of system components (i.e., from offshore, SAB, gap region to berm) to various driving forces, to provide details of hydrodynamics and sediment transport, and to analysis the morphological and hydrodynamical coupling of each component. On the other hand, details of type and composition of all available sediment sources in the area seaward of the SAB, in and around the SAB itself, and in the gap-area will be investigated in the follow-up studies.

5. Conclusions

Laboratory experiments are carried out to investigate the SAB beach profile evolution under the storm wave condition, considering different shapes of background profiles and various SAB designs. The responses of the SAB and the berm as well as their morphological coupling, are of special interest. The results lead to the following conclusions:

- 1) On the reflective beach, onshore migration of the SAB and the berm shape movement are observed. The SAB with a smaller crest depth protects the berm better under storm wave conditions. On the intermediate beach, the SAB is merged with the outer sandbar, promoting inner bar onshore migration and berm formation. By analyzing net sediment transport patterns, it has been found that the beach state is altered by the SAB which triggers onshore sediment transport locally. SAB placed on natural sandbar trough is more efficient in reducing erosion than that implemented on seaward of natural sandbar.
- 2) Under large wave conditions, the SAB responds differently to natural sandbars due to its unnaturally steep slope and small water depth over the crest. It is observed that SAB migrates onshore with bar height decreasing and both slopes becoming mild. Bar height and both slopes show a rapid decrease in the beginning, and then tend to be stable. The concept of half-life period is proposed to indicate SAB

- stability. The half-life period of SAB is influenced by its seaward slope and the relative crest water depth, which are both time-varying.
- 3) Berm rollover shows an equilibrium trend after initially sharp decreasing. A dimensionless parameter is proposed to describe the temporal evolution of the berm shape. A morphological coupling is found between the SAB and berm, and the response of the berm to storm waves is affected by the morphology of the SAB, indicating that the lee effect of the SAB is dynamic. On that basis, an empirical relationship has been proposed to quantitatively describe the strong morphological coupling of SAB and berm.
- 4) The experiment results are used to validate a process-based numerical beach evolution model. The model predicts beach profile evolution on the intermediate beach well, but fails to reproduce the onshore bar migration on the reflective beach. This is probably because the phase coupling between the moment of injection of plunging jets into bottom and the timing of wave crest is not considered in the model. The modelled wave energy dissipation induced by the SAB is found to be related to both the morphology of the SAB and berm. The finding explains the morphological coupling from the perspective of the wave energy dissipation, and provides direct evidence that the SAB protects the rear beach berm by weakening wave energy.
- 5) Although the findings in this study are obtained from an idealized wave flume experiment, it provides a possibility to use such type of the SAB to prevent severe erosion under storm conditions, and provides useful datasets for further calibration of the numerical model. Future works will be carried out using a comprehensive 3D integrated numerical model to reveal the morphological responses of the beach system with the SAB to various driving forces, and investigating details of type and composition of all available sediment sources in the area seaward of the SAB, in and around the SAB itself, and in the gap-area.

Data availability

The data supporting the findings in this paper has been uploaded in Mendeley Database, <https://doi.org/10.17632/n59hc4r3n.1>.

Declaration of Competing Interest

The authors declare that they have no known competing financial interests or personal relationships that could have appeared to influence the work reported in this paper.

Acknowledgments

The comments from two reviewers are highly appreciated. Our students Yu Cai and Haoye Yang are acknowledged for their contributions in conducting experiments. This work was supported by the National Natural Science Foundation of China (51879096), the Key Program of National Natural Science Foundation of China (41930538), National Natural Science Foundation of China (51909076) and the Special Research Funding of State Key Laboratory of Hydrology-Water Resources and Hydraulic Engineering (20195025812, 20185044512).

References

- Aagaard, T., 2014. Sediment supply to beaches: Cross-shore sand transport on the lower shoreface. *J. Geophys. Res. Earth Surf.* 119, 913–926.
- Aagaard, T., Hughes, M.G., Ruessink, G., 2018. Field Observations of Turbulence, Sand Suspension, and Cross-Shore Transport under Spilling and Plunging Breakers. *J. Geophys. Res. Earth Surf.* 123 (11), 2844–2862.
- Alsina, J.M., Cáceres, I., Brocchini, M., Baldock, T.E., 2012. An experimental study on sediment transport and bed evolution under different swash zone morphological conditions. *Coast. Eng.* 68, 31–43.
- Atkinson, A.L., Baldock, T.E., 2020. Laboratory investigation of nourishment options to mitigate sea level rise induced erosion. *Coast. Eng.* 161, 103769.
- Atkinson, A.L., Baldock, T.E., Birrien, F., Callaghan, D.P., Nielsen, P., Beuzen, T., Turner, I.L., Blenkinsopp, C.E., Ranasinghe, R., 2018. Laboratory investigation of the Bruun Rule and beach response to sea level rise. *Coast. Eng.* 136, 183–202.
- Baldock, T.E., Holmes, P., Bunker, S., Van Weert, P., 1998. Cross-shore hydrodynamics within an unsaturated surf zone. *Coast. Eng.* 34 (3–4), 173–196.
- Baldock, T.E., Alsina, J.A., Cáceres, I., Vicinanza, D., Contestabile, P., Power, H., Sanchez-Arcilla, A., 2011. Large-scale experiments on beach profile evolution and surf and swash zone sediment transport induced by long waves, wave groups and random waves. *Coast. Eng.* 58 (2), 214–227.
- Baldock, T.E., Birrien, F., Atkinson, A., Shimamoto, T., Wu, S., Callaghan, D.P., Nielsen, P., 2017. Morphological hysteresis in the evolution of beach profiles under sequences of wave climates - part 1; observations. *Coast. Eng.* 128, 92–105.
- Baldock, T.E., Gravois, U., Callaghan, D.P., Davies, G., Nichol, S., 2021. Methodology for estimating return intervals for storm demand and dune recession by clustered and non-clustered morphological events. *Coast. Eng.* 168, 103924.
- Battjes, J.A., 1974. Surf similarity. In: Proceedings of International Conference on Coastal Engineering, pp. 466–480.
- Camus, P., Losada, I.J., Izaguirre, C., Espejo, A., Menéndez, M., Pérez, J., 2017. Statistical wave climate projections for coastal impact assessments. *Earth's Future* 5 (9), 918–933.
- Chen, W.L., Dodd, N., 2019. An idealised study for the evolution of a shoreface nourishment. *Cont. Shelf Res.* 178, 15–26.
- Chen, D., Wang, Y., Melville, B., Huang, H., Zhang, W., 2018. Unified Formula for critical Shear stress for Erosion of sand, Mud, and Sand Mud Mixtures. *J. Hydraul. Eng.* 144, 04018046.
- Chen, D., Melville, B., Zheng, J., Wang, Y., Zhang, C., Guan, D., Chen, C., 2021. Pickup rate of non-cohesive sediments in low-velocity flows. *J. Hydraul. Res.* <https://doi.org/10.1080/00221686.2020.1871430>.
- Coco, G., Senechal, N., Rejas, A., Bryan, K.R., Capo, S., Parisot, J.P., Brown, J.A., MacMahon, J.H.M., 2014. Beach response to a sequence of extreme storms. *Geomorphology* 204, 493–501.
- Cooke, B.C., Jones, A.R., Goodwin, I.D., Bishop, M.J., 2012. Nourishment practices on Australian sandy beaches: a review. *J. Environ. Manag.* 113, 319–327.
- Dalrymple, R.A., 1992. Prediction of storm/normal beach profiles. *J. Waterw. Port Coast. Ocean Eng.* 118 (2), 193–200.
- de Schipper, M., Ludka, B., Raubenheimer, B., Luijendijk, A., Schlacher, A.T., 2020. Beach nourishment has complex implications for the future of sandy shores. *Nature Rev. Earth Environ.* 2 (1), 70–84.
- Dean, R.G., 1977. Equilibrium Beach Profiles: US Atlantic and Gulf Coasts. Department of Civil Engineering and College of Marine Studies, University of Delaware.
- Dissanayake, P., Brown, J., Wisse, P., Karunarathna, H., 2015. Effects of storm clustering on beach/dune evolution. *Mar. Geol.* 370, 63–75.
- Eichentopf, S., Karunarathna, H., Alsina, J.M., 2019. Morphodynamics of sandy beaches under the influence of storm sequences: current research status and future needs. *Water Sci. Eng.* 12 (3), 221–234.
- Eichentopf, S., Alsina, J.M., Christou, M., Kuriyama, Y., Karunarathna, H., 2020a. Storm sequencing and beach profile variability at Hasaki, Japan. *Mar. Geol.* 424, 106153.
- Eichentopf, S., van der Zanden, J., Cáceres, I., Baldock, T.E., Alsina, J.M., 2020b. Influence of storm sequencing on breaker bar and shoreline evolution in large-scale experiments. *Coast. Eng.* 157, 103659.
- Elko, N.A., 2006. Storm-influenced sediment transport gradients on a nourished beach. Ph.D thesis. University of South Florida, USA.
- Fan, J., Zheng, J., Tao, A., Liu, Y., 2021. Upstream-propagating waves induced by steady current over a rippled bottom: theory and experimental observation. *J. Fluid Mech.* 910, A49.
- Gourlay, M.R., 1968. Beach and Dune Erosion Report M935/M936 (Delft Hydraulics Laboratory).
- Grasso, F., Michallet, H., Barthélémy, E., 2011. Experimental simulation of shoreface nourishments under storm events: A morphological, hydrodynamic, and sediment grain size analysis. *Coast. Eng.* 58 (2), 184–193.
- Grunnet, N.M., Ruessink, B.G., 2005. Morphodynamic response of nearshore bars to a shoreface nourishment. *Coast. Eng.* 52 (2), 119–137.
- Grunnet, N.M., Walstra, D.J.R., Ruessink, B.G., 2004. Process-based modelling of a shoreface nourishment. *Coast. Eng.* 51 (7), 581–607.
- Guimaraes, A., Coelho, C., Veloso-Gomes, F., Silva, P.A., 2021. 3D Physical Modeling of an Artificial Beach Nourishment: Laboratory Procedures and Nourishment Performance. *J. Mar. Sci. Eng.* 9, 613.
- Hamm, L., Capobianco, M., Dette, H., Lechuga, A., Spanhoff, R., Stive, M., 2002. A summary of European experience with shore nourishment. *Coast. Eng.* 47 (2), 237–264.
- Hattori, M., Kawamata, R., 1980. Onshore-offshore transport and beach profile change. In: *Proceedings of the 17th Coastal Engineering Conference. ASCE*, pp. 1175–1193.
- Hearin, J., 2014. Historical analysis of beach nourishment and its impact on the morphological modal beach state in the North Reach of Brevard County, Florida. *Coastal Mar. Res.* 2 (3), 37–53.
- Holman, R.A., Lalejini, D.M., Edwards, K., Veeramony, J., 2014. A parametric model for barred equilibrium beach profiles. *Coast. Eng.* 90, 85–94.
- Holman, R.A., Lalejini, D.M., Holland, T., 2016. A parametric model for barred equilibrium beach profiles: two-dimensional implementation. *Coast. Eng.* 117, 166–175.
- Hughes, S.A., 1993. *Physical Models and Laboratory Techniques in Coastal Engineering*. Advances Series on Coastal Engineering. World Scientific Publishing, Singapore.
- Huisman, B.J.A., Walstra, D.J.R., Rademacher, M., de Schipper, M.A., Ruessink, B.G., 2019. Observations and Modelling of Shoreface Nourishment Behaviour. *J. Mar. Sci. Eng.* 7, 59.
- Jackson, D., Short, A., 2020. *Sandy Beach Morphodynamics*. Elsevier.

- Jacobsen, N.G., Fredsøe, J., 2014. Cross-Shore Redistribution of Nourished Sand near a Breaker Bar. *J. Waterw. Port Coast. Ocean Eng.* 140 (2), 125–134.
- Janssen, T.T., Battjes, J.A., 2007. A note on wave energy dissipation over steep beaches. *Coast. Eng.* 54, 711–716.
- Kuang, C., Han, X., Zhang, J., Zou, Q., Dong, B., 2021. Morphodynamic Evolution of a Nourished Beach with Artificial Sandbars: Field Observations and Numerical Modeling. *J. Mar. Sci. Eng.* 9, 245.
- Larson, M., Hanson, H., 2015. Model of the evolution of mounds placed in the nearshore. *J. Integr. Coastal Zone Manag.* 21–33.
- Li, Y., Zhang, C., Chen, D., Zheng, J., Sun, J., Wang, P., 2021a. Barred beach profile equilibrium investigated with a process-based numerical model. *Cont. Shelf Res.* 222, 104432.
- Li, Y., Zhang, C., Cai, Y., Xie, M., Qi, H., Wang, Y., 2021b. Wave Dissipation and Sediment Transport patterns during Shoreface Nourishment towards Equilibrium. *J. Mar. Sci. Eng.* 9 (5), 535.
- Liu, G., Cai, F., Qi, H., Zhu, J., Liu, J., 2019a. Morphodynamic evolution and adaptability of nourished beaches. *J. Coast. Res.* 35 (4), 737–750.
- Liu, B., Cheng, D., Sun, Z., Zhao, X., Cheng, Y., Lin, W., 2019b. Experimental and numerical study of regular waves past a submerged breakwater. *J. Hydron.* 31 (4), 641–653.
- Luijendijk, A.P., Ranasinghe, R., de Schipper, M.A., Huisman, B.A., Swinkels, C.M., Walstra, D.J.R., Stive, M.J.F., 2017. The initial morphological response of the Sand Engine: A process-based modelling study. *Coast. Eng.* 119, 1–14.
- Luo, S., Cai, F., Liu, H., Lei, G., Qi, H., Su, X., 2015. Adaptive measures adopted for risk reduction of coastal erosion in the People's Republic of China. *Ocean Coast. Manag.* 103, 134–145.
- Marinho, B., Coelho, C., Larson, M., Hanson, H., 2020. Cross-shore modelling of multiple nearshore bars at a decadal scale. *Coast. Eng.* 159, 103722.
- Masselink, G., Beetham, E., Kench, P., 2020. Coral reef islands can accrete vertically in response to sea level rise. *Sci. Adv.* 6 eaay3656.
- McFall, B.C., Brutsché, K.E., Priestas, A.M., Krafft, D.R., 2021. Evaluation technique for the beneficial use of dredged sediment placed in the nearshore. *J. Waterw. Port Coast. Ocean Eng.* 147 (5), 04021016.
- Murray, A.B., Lazarus, E., Ashton, A., Baas, A., Coco, G., Coulthard, T., Fonstand, M., Haff, P., McNamara, D., Paola, C., Pelletier, J., Reinhardt, L., 2009. Geomorphology, complexity, and the emerging science of the earth's surface. *Geomorphology* 103, 456–505.
- Nielsen, P., Shimamoto, T., 2015. Bar response to tides under regular waves. *Coast. Eng.* 106, 1–3.
- Pan, Y., Kuang, C., Zhang, J., Chen, Y., Mao, X., Ma, Y., Zhang, Y., Yang, Y., Qiu, R., 2017. Postnourishment evolution of beach profiles in a low-energy sandy beach with a submerged Berm. *J. Waterw. Port Coast. Ocean Eng.* 143 (4), 05017001.
- Pietro, L.S., O'Neal, M.A., Puleo, J.A., 2008. Developing terrestrial-LIDAR-based digital elevation models for monitoring beach nourishment performance. *J. Coast. Res.* 24 (6), 1555–1564.
- Price, T., Ruessink, B.G., 2011. State dynamics of a double sandbar system. *Cont. Shelf Res.* 31 (6), 659–674.
- Rafati, Y., Hsu, T.J., Elgar, S., Raubenheimer, B., Quataert, E., van Dongeren, A., 2021. Modeling the hydrodynamics and morphodynamics of sandbar migration events. *Coast. Eng.* 166, 103885.
- Roelvink, D., Costas, S., 2017. Beach berms as an essential link between subaqueous and subaerial beach/dune profiles. *Geotemas* 17, 79–82.
- Roman-Sierra, J., Munoz-Perez, J.J., Navarro-Pons, M., 2014. Beach nourishment effects on sand porosity variability. *Coast. Eng.* 83, 221–232.
- Ruessink, B., Walstra, D., Southgate, H., 2003. Calibration and verification of a parametric wave model on barred beaches. *Coast. Eng.* 48 (3), 139–149.
- Ruessink, B.G., Kuriyama, Y., Reniers, A.J.H.M., Roelvink, J.A., Walstra, D.J.R., 2007. Modeling cross-shore sandbar behavior on the timescale of weeks. *J. Geophys. Res. Earth Surf.* 112, F03010.
- Ruggiero, P., Kaminsky, G.M., Gelfenbaum, G., Cohn, N., 2016. Morphodynamics of prograding beaches: A synthesis of seasonal- to century-scale observations of the columbia river littoral cell. *Mar. Geol.* 376, 51–68.
- Sanchez-Arcilla, A., Caceres, I., 2017. An analysis of nearshore profile and bar development under large scale erosive and accretive waves. *J. Hydraul. Res.* 56 (2), 231–244.
- Schoonees, T., Gijón Mancheno, A., Scheres, B., Bouma, T.J., Silva, R., Schlurmann, T., Schütttrumpf, H., 2019. Hard Structures for Coastal Protection, Towards Greener designs. *Estuar. Coasts* 42 (7), 1709–1729.
- Scott, C.P., Cox, D.T., Shin, S., Clayton, N., 2004. Estimates of surf zone turbulence in a large-scale laboratory flume. Proceedings of the. In: 29th Conference on Coastal Engineering, ASCE, pp. 379–391.
- Short, A.D., Hesp, P.A., 1982. Wave, beach and dune interactions in southeastern Australia. *Mar. Geol.* 48 (3–4), 259–284.
- Smith, E.R., Mohr, M.C., Chader, S.A., 2017. Laboratory experiments on beach change due to nearshore mound placement. *Coast. Eng.* 121, 119–128.
- Spielmann, K., Certain, R., Astruc, D., Barusseau, J.P., 2011. Analysis of submerged bar nourishment strategies in a wave-dominated environment using a 2DV process-based model. *Coast. Eng.* 58 (8), 767–778.
- Sui, T., Staunstrup, L.H., Carstensen, S., Fuhrman, D.R., 2021. Span shoulder migration in three-dimensional current-induced scour beneath submerged pipelines. *Coast. Eng.* 164, 103776.
- Toimil, A., Losada, I.J., Nicholls, R.J., Dalrymple, R.A., Stive, M.J.F., 2020. Addressing the challenges of climate change risks and adaptation in coastal areas: A review. *Coast. Eng.* 156, 103611.
- van der Meer, J.W., Brigandt, R., Zanuttigh, B., Wang, B., 2005. Wave transmission and reflection at low-crested structures: Design formulae, oblique wave attack and spectral change. *Coast. Eng.* 52 (10–11), 915–929.
- van der Werf, J.J., de Vet, P.L.M., Boersma, M.P., Bouma, T.J., Nolte, A.J., Schrijvershof, R.A., Ysebaert, T., 2019. An integral approach to design the Roggenplaat intertidal shoal nourishment. *Ocean Coast. Manag.* 172, 30–40.
- van der Westhuysen, A.J., 2010. Modeling of depth-induced wave breaking under finite depth growth conditions. *J. Geophys. Res. Oceans* 115, C01008.
- van der Zanden, J., van der A, D. A., Cáceres, I., Hurther, D., McLelland, S. J., Ribberink, J. S., and O'Donoghue, T., 2018. Near-bed turbulent kinetic energy budget under a large-scale plunging breaking wave over a fixed bar. *J. Geophys. Res. Oceans* 123 (2), 1429–1456.
- van der Zanden, J., Van Der, A., Hurther, D., Cáceres, I., O'Donoghue, T., Ribberink, J., 2016. Near-bed hydrodynamics and turbulence below a large-scale plunging breaking wave over a mobile barred bed profile. *J. Geophys. Res. Oceans* 121 (8), 6482–6506.
- Van Der, A.D., Van Der Zanden, J., O'Donoghue, T., Hurther, D., Cáceres, I., McLelland, S.J., Ribberink, J.S., 2017. Large-scale laboratory study of breaking wave hydrodynamics over a fixed bar. *J. Geophys. Res. Oceans* 122 (4), 3287–3310.
- van Duin, M.J.P., Wiersma, N.R., Walstra, D.J.R., van Rijn, L.C., Stive, M.J.F., 2004. Nourishing the shoreface: observations and hindcasting of the Egmond case, the Netherlands. *Coast. Eng.* 51, 813–837.
- van Rijn, L., Walstra, D., Grasmeijer, B., Sutherland, J., Pan, S., Sierra, J., 2003. The predictability of cross-shore bed evolution of sandy beaches at the time scale of storms and seasons using process-based profile models. *Coast. Eng.* 47 (3), 295–327.
- Voudoukas, M.I., Almeida, L.P.M., Ferreira, O., 2012. Beach erosion and recovery during consecutive storms at a steep-sloping, meso-tidal beach. *Earth Surf. Process. Landf.* 37, 583–593.
- Voudoukas, M.I., Mentaschi, L., Voukouvalas, E., Verlaan, M., Jevrejeva, S., Jackson, L. P., Feyen, L., 2018. Global probabilistic projections of extreme sea levels show intensification of coastal flood hazard. *Nat. Commun.* 9 (1), 2360.
- Walstra, D.J.R., Hooyng, C.W., Tonnon, P.K., Van Rijn, L.C., 2011. Experimental Study investigating various Shoreface Nourishment designs. *Coastal Eng Proceed.* 1 (32).
- Wengrove, M., 2018. Bedform Geometry and Bedload Sediment Flux in Coastal Wave, Current, and Combined Wave-Current Flows. Doctoral Dissertations, University of New Hampshire, Durham.
- Winter, C., Vittori, G., Ernstsen, V.B., Bartholdy, J., 2008. On the Superimposition of Bedforms in Tidal Channels (Marlene and River Dune Dynamics).
- Wright, L.D., Short, A.D., 1984. Morphodynamic variability of surf zones and beaches: a synthesis. *Mar. Geol.* 56 (1–4), 93–118.
- Wright, L.D., Short, A.D., Green, M., 1985. Short-term changes in the morphodynamic states of beaches and surf zones: an empirical predictive model. *Mar. Geol.* 62 (3–4), 339–364.
- Xing, Y., Shao, D., Yang, Y., Ma, X., Zhang, S., 2021. Influence and interactions of input factors in urban flood inundation modeling: an examination with variance-based global sensitivity analysis. *J. Hydrol.* 600 (2), 126524.
- Xue, M., Zheng, J., Lin, P., Yuan, X., 2017. Experimental study on vertical baffles of different configurations in suppressing sloshing pressure. *Ocean Eng.* 136, 178–189.
- Yuksel, Z.T., Kobayashi, N., 2020. Comparison of Revetment and Sill in reducing Shore Erosion and Wave Overtopping. *J. Waterw. Port Coast. Ocean Eng.* 146 (1), 04019028.
- Zhang, C., Zhang, Q., Zheng, J., Demirbilek, Z., 2017. Parameterization of nearshore wave front slope. *Coast. Eng.* 127, 80–87.
- Zhang, C., Li, Y., Cai, Y., Shi, J., Zheng, J., Cai, F., Qi, H., 2021a. Parameterization of nearshore wave breaker index. *Coast. Eng.* 168, 103914.
- Zhang, C., Li, Y., Zheng, J., Xie, M., Shi, J., Wang, G., 2021b. Parametric modelling of nearshore wave reflection. *Coast. Eng.* 169, 103978.
- Zheng, J., Zhang, C., Demirbilek, Z., Lin, L., 2014. Numerical study of sandbar migration under wave-undertow interaction. *J. Waterw. Port Coast. Ocean Eng.* 140 (2), 146–159.
- Zheng, J., Yao, Y., Chen, S.G., Chen, S.B., Zhang, Q., 2020. Laboratory study on wave-induced setup and wave-driven current in a 2DH reef-lagoon-channel system. *Coast. Eng.* 162, 103772.
- Zhu, T., Kobayashi, N., 2021. Rock mound to reduce wave overwash and crest lowering of a sand barrier. *Coast. Eng. J.* <https://doi.org/10.1080/21664250.2021.1957550>.